Corrected 15 September 2018. See full text.

METAMATERIALS

Quantum entanglement of the spin and orbital angular momentum of photons using metamaterials

Tomer Stav[1]*, Arkady Faerman[2]*, Elhanan Maguid[2], Dikla Oren[1], Vladimir Kleiner[2], Erez Hasman[2]†, Mordechai Segev[1]†

Metamaterials constructed from deep subwavelength building blocks have been used to demonstrate phenomena ranging from negative refractive index and ε-near-zero to cloaking, emulations of general relativity, and superresolution imaging. More recently, metamaterials have been suggested as a new platform for quantum optics. We present the use of a dielectric metasurface to generate entanglement between the spin and orbital angular momentum of photons. We demonstrate the generation of the four Bell states on a single photon by using the geometric phase that arises from the photonic spin-orbit interaction and subsequently show nonlocal correlations between two photons that interacted with the metasurface. Our results show that metamaterials are suitable for the generation and manipulation of entangled photon states, introducing the area of quantum optics metamaterials.

Metamaterials are engineered structures, assembled from multiple elements of a scale smaller than the wavelength of incident light, with distinct electromagnetic response and functionalities such as negative refraction (*1*, *2*), cloaking (*3*), and even near-zero permittivity and permeability (*4*, *5*). Metasurfaces consist of a dense arrangement of dielectric or metallic subwavelength optical antennas (*6*–*14*). The light-matter interaction of an individual nanoantenna provides control over the local phase (*15*), enabling control over refraction and reflection. Accordingly, the light-scattering properties of the metasurface can be manipulated by tailoring the nanoantennas' material, size, and shaping the antenna resonance (*9*, *13*, *14*), or through their arrangement in space—for example, with geometric phase (*6*, *7*, *12*). These wavefront manipulations have been widely used with classical light. Recently, a metallic metasurface was used with quantum light (*16*) for detecting coherent perfect absorption of single photons. In this context, interesting ideas on how to utilize metamaterials for creating entanglement have been proposed (*17*). However, metamaterials have never been used to generate or manipulate entangled photon states, which are at the heart of the field of photonic quantum information.

By exploiting fundamental concepts in quantum physics, such as superposition and entanglement, quantum information offers ways of solving problems in reduced time-complexity (*18*–*20*). One of the many possible realizations of quantum algorithms may be achieved by using single photons encoded with two qubits (*21*), whose relatively easy manipulation makes the construction of optical quantum processing units appealing. This is because photons can be controlled with the same optical devices used for classical light; they maintain their quantum coherence (quantum correlations) for extremely long times, unless absorbed (*22*–*24*). That is, they do not suffer from severe decoherence problems, as the alternative platforms to quantum information do. Indeed, recent advancements in on-chip quantum photonic circuits have shown the benefits of having integrated entangled photon sources (*25*, *26*). Several experiments involving entangled photon states and metamaterials have been performed (*27*, *28*); however, thus far the entangled photon states were generated before the interaction with the metamaterial. Moreover, for experiments with quantum light, it is important to minimize the loss, whereas metallic metasurfaces inherently exhibit high loss (*28*). We used metasurfaces made of high-refractive index dielectrics, which do not involve any plasmonic decoherence or loss. Moreover, our dielectric metasurfaces are compatible with complementary metal-oxide semiconductor technology in the fabrication process, which is advantageous for future large-scale quantum computation devices. We rely on the recent realizations of Si-based metasurfaces with efficiencies close to 100% (*14*, *29*), which makes them excellent candidates for quantum optics and quantum information applications.

We demonstrate that a dielectric metasurface can generate entanglement between the spin and the orbital angular momentum (OAM) of photons (Fig. 1). This is achieved by using the Pancharatnam-Berry phase, which provides a photonic spin-orbit interaction mechanism (*30*–*32*). We fabricated the Si-based geometric phase metasurface (GPM) depicted in Fig. 2A. In general, GPMs are designed for spin-controlled wave function shaping and are composed of anisotropic nanoantennas, designed to perform as nano half-waveplates, that generate a local geometric phase delay. The space-variant spin-dependent geometric phase $\phi_g(x, y) = -2\sigma_{\pm}\theta(x, y)$ corresponds to the orientation function $\theta(x, y)$ and defines the phase of the light passing through the metasurface at position (x, y) for the different spin states $\sigma_{\pm} = \pm 1$ (right- and left-handed circular polarizations). The angle $\theta(x, y)$ is the in-plane orientation of the nanoantennas. To design a GPM that entangles the photon's spin to its OAM, the nanoantenna orientations are chosen to be $\theta(r, \varphi) = \ell\varphi/2$, where φ is the azimuthal angle and ℓ is the winding number; in our case, $\ell = 1$. Therefore, the GPM adds or subtracts $\Delta\ell = 1$—one

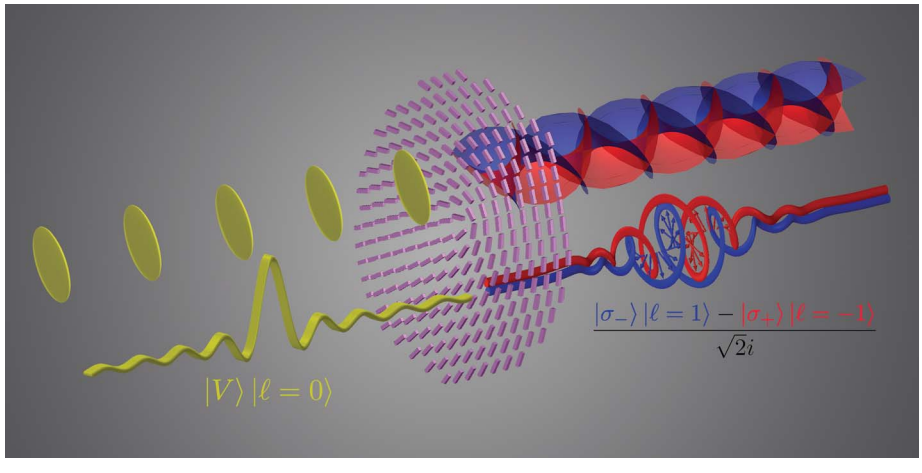

Fig. 1. Entanglement between spin and OAM on a single photon. A single photon vertically polarized is arriving from the left, as illustrated by the yellow wave packet representing the electric field amplitude. This photon carries zero OAM, as illustrated by the yellow flat phase fronts. The single photon passes through the metasurface nanoantennas (purple) and exits as a single-particle entangled state, depicted as a superposition of the red and blue electric field amplitudes, with the corresponding vortex phase fronts opposite to one another.

[1]Physics Department and Solid State Institute, Technion, Haifa 32000, Israel. [2]Micro and Nanooptics Laboratory, Faculty of Mechanical Engineering, and Russell Berrie Nanotechnology Institute, Technion, Haifa 32000, Israel.
*These authors contributed equally to this work.
†Corresponding author. Email: mehasman@technion.ac.il (E.H.); msegev@technion.ac.il (M.S.)

Downloaded from http://science.sciencemag.org/ on September 16, 2018

Corrected 15 September 2018. See full text.

quanta of OAM, depending on the sign of the spin—and performs spin-flip $|\sigma_+\rangle \leftrightarrow |\sigma_-\rangle$. Such a metasurface performs the unitary transformation

$$|\sigma_\pm\rangle|\ell\rangle \overset{\text{GPM}}{\rightleftarrows} |\sigma_\mp\rangle|\ell \pm \Delta\ell\rangle \quad (1)$$

A single photon with zero OAM, polarized horizontally (H), incident upon the metasurface can be described by a superposition of spins (circular polarizations) as

$$|H\rangle|\ell = 0\rangle = \frac{1}{\sqrt{2}}(|\sigma_+\rangle + |\sigma_-\rangle)|\ell = 0\rangle \quad (2)$$

After passing through the metasurface, the state of the photon becomes (following Eq. 1)

$$\frac{1}{\sqrt{2}}(|\sigma_-\rangle|\ell = \Delta\ell\rangle + |\sigma_+\rangle|\ell = -\Delta\ell\rangle) \quad (3)$$

Similarly, an incident photon with zero OAM in the vertical polarization (V), described by $|V\rangle|\ell = 0\rangle = \frac{1}{\sqrt{2}i}(|\sigma_+\rangle - |\sigma_-\rangle)|\ell = 0\rangle$, is transformed by the metasurface into

$$\frac{1}{\sqrt{2}i}(|\sigma_-\rangle|\ell = \Delta\ell\rangle - |\sigma_+\rangle|\ell = -\Delta\ell\rangle) \quad (4)$$

The states described by Eqs. 3 and 4 are maximally entangled states encoded on a single photon. The entanglement here is between the spin and the OAM degrees of freedom. In a similar fashion, following Eqs. 3 and 4, if two indistinguishable photons in the state $|H\rangle|\ell = 0\rangle \otimes |V\rangle|\ell = 0\rangle$ are passed through the GPM, the result is the state

$$\frac{1}{\sqrt{2}}(|\sigma_+\rangle|\ell = -1\rangle \otimes |\sigma_+\rangle|\ell = -1\rangle - |\sigma_-\rangle|\ell = 1\rangle \otimes |\sigma_-\rangle|\ell = 1\rangle) \quad (5)$$

Both the spin and the OAM represent angular momentum, and only their sum is conserved (*33*). Nevertheless, for photons whose spatial wave function is paraxial, as in our case, the spin and the OAM are totally independent (*32*) and have Hilbert spaces of different dimensions. Furthermore, from expectation value perspective, the total angular momentum is conserved; the incident state is of zero total angular momentum as well as the state emerging from the GPM.

The experimental setting shown in Fig. 2B is used to generate a single photon in the state $|H\rangle|\ell = 0\rangle$. In the first set of experiments, the interaction with the metasurface results in a single

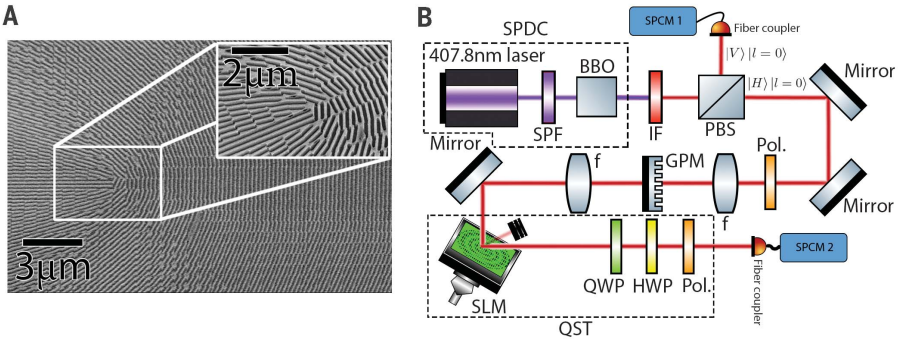

Fig. 2. Experimental setup used to generate and measure the entangled states. (**A**) Scanning electron microscope image of the Si-based GPM. Each building block in the GPM is composed of several nanorods filling an area of 700 by 700 nm^2. The nanorods are of 105 nm width and 300 nm depth, arranged 233 nm apart from each other. The metasurface diameter is 200 μm. (**B**) Schematic of the experimental setup. A 407.8-nm diode laser pumps a β-barium borate (BBO) crystal phase-matched for type-II collinear spontaneous parametric down-conversion (SPDC). The SPDC process produces two photons, one in vertical polarization (V) and the other in horizontal polarization (H), centered around the degenerate wavelength of λ = 815.6 nm. The pump field and photons produced at other wavelengths are filtered out by an interference filter (IF) filter. The pairs of photons produced by means of SPDC are spatially separated by using a polarizing beam splitter (PBS). The reflected photon acts as a trigger for the detection of the "signal photon" in H polarization (Eq. 2). The signal photon is passed through a linear polarizer (Pol.) and then through the GPM. In the measurement process, this single photon is reflected off a phase-only SLM that projects the state onto different OAM bases. Then the photons are projected on different polarization bases and measured in the SPCMs. Coincidence counts between the two SPCMs are used to measure different intensities for the QST.

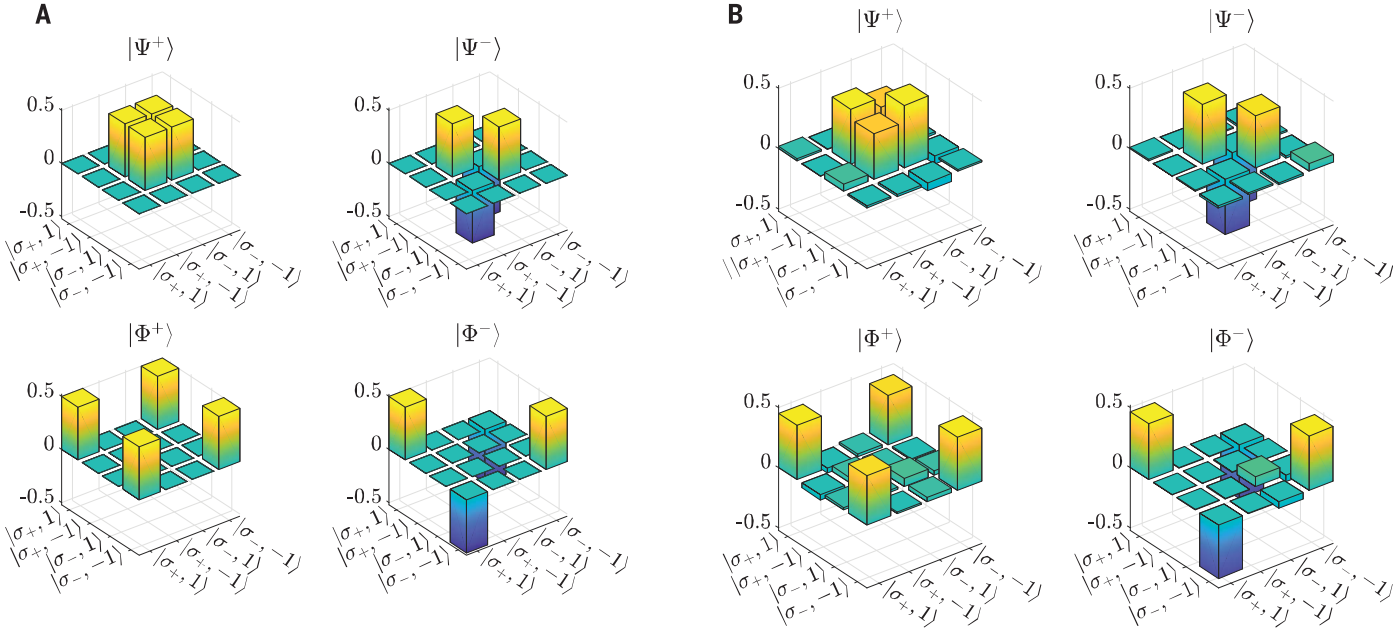

Fig. 3. Density matrices of the four Bell states. (**A**) Theoretical calculated density matrices for each Bell state. (**B**) Experimentally measured density matrices recovered for each Bell state by using QST. The experimental results coincide with the theoretical results with higher than 90% fidelity. The results shown here are the real parts only because the imaginary part is identically zero both theoretically and experimentally.

Downloaded from http://science.sciencemag.org/ on September 16, 2018

Corrected 15 September 2018. See full text.

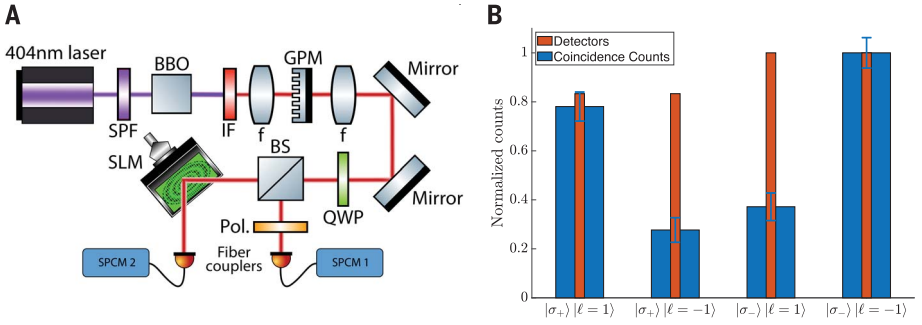

Fig. 4. Setup and measurements demonstrating nonlocal spin and OAM correlations on entangled biphoton states. (**A**) A 404-nm diode laser pumps a BBO crystal phase-matched for collinear type-II SPDC, which produces two photons in the degenerate wavelength of λ = 808 nm, filtered with an IF of $\Delta\lambda$ = 3 nm. The pairs of photons are passed together through the GPM. After the interaction with the GPM, the photons pass through a QWP and into a BS. The reflected photons are projected on linear polarization states H and V, and the transmitted photons are projected on OAM states $\ell = \pm 1$. Coincidence counts between the two SPCMs are used to measure the nonlocal correlations between the two photons. (**B**) Coincidence counts measured between the two arms of the BS. The correlation between the linear polarization of one photon and the OAM of the second photon shows entanglement between the spin and OAM of two different photons. The uncorrelated terms are not zero because the metasurface we used was measured to have 72% conversion efficiency, decreasing the visibility in this case.

photon in an entangled state. In the second set of experiments, the metasurface generates entangled biphoton states. The experimental conversion efficiency of the metasurface was measured to be 72%.

To show entanglement, we performed full quantum state tomography (QST) on the state, and the density matrix is recovered (*34*). We used a spatial light modulator (SLM) to project the state onto different OAM basis elements, and a set of quarter-waveplate (QWP), half-waveplate (HWP) and a linear polarizer (Pol.) to project the state onto different elements of the polarization basis. The list of measurements is described in table S1. We used coincidence counts between the two detectors so that the single photon state is heralded. For integration time of 10 s, ~1000 coincidence counts were measured without any projections. From a total of 16 different measurements for each of the Bell states, we recovered the density matrix using a maximum likelihood estimation algorithm (*35*). Using this technique, we experimentally recovered the density matrices of the first two bell states $|\Psi^{\pm}\rangle = \frac{1}{\sqrt{2}}(|\sigma_+\rangle|\ell=-1\rangle \pm |\sigma_-\rangle|\ell=1\rangle)$ with fidelity of 0.9250 and 0.9496 for $|\Psi^{+}\rangle$ and $|\Psi^{-}\rangle$, respectively (Fig. 3B), where we define the fidelity between the recovered ($\tilde{\rho}$) and theoretical (ρ) density matrices by $F(\rho,\tilde{\rho}) = \mathrm{Tr}\left(\sqrt{\tilde{\rho}^{1/2}\rho\tilde{\rho}^{1/2}}\right)$. By flipping the GPM (the winding number flips sign, and now $\ell = -1$), it performs the unitary transformation $|\sigma_{\pm}\rangle|\ell\rangle \overset{\mathrm{GPM}}{\rightleftarrows} |\sigma_{\mp}\rangle|\ell \mp \Delta\ell\rangle$, which enables the generation of the remaining two bell states $|\Phi^{\pm}\rangle = \frac{1}{\sqrt{2}}(|\sigma_+\rangle|\ell=1\rangle \pm |\sigma_-\rangle|\ell=-1\rangle)$. We performed QST on these states and measured density matrices with fidelity of 0.9274 and 0.9591 for $|\Phi^{+}\rangle$ and $|\Phi^{-}\rangle$, respectively (Fig. 3B). These results are in very good agreement with theory (Fig. 3A). By introducing a HWP after the GPM, we can realize a SWAP gate on the spin qubit $|\sigma_+\rangle|\ell\rangle \overset{\mathrm{SWAP}}{\rightleftarrows} |\sigma_-\rangle|\ell\rangle$, performing the transformation $|\Phi^{\pm}\rangle \overset{\mathrm{SWAP}}{\rightleftarrows} |\Psi^{\pm}\rangle$. This SWAP gate does not affect the OAM qubit, which remains independent from the spin qubit (with fidelity 0.9276) (fig. S1).

Next, we demonstrate nonlocal spin and OAM correlations between two photons, using the experimental setting described in Fig. 4A. Coincidence counts between the two single-photon counting modules (SPCMs) measure correlations only half the times, when the two photons exit the beam splitter in different arms. The results displayed in Fig. 4B show that the emerging state manifests correlations between the spin of one photon and OAM of the other photon, which cannot be reproduced with classical light. The conclusion drawn from the single-photon state tomography (Fig. 3B) and the correlation measurements between two photons (Fig. 4B) is that the metasurface does not destroy the coherence of the wave function and generates entanglement between the spin and OAM at high fidelity.

Our demonstration of generating entangled photon states with metamaterials paves the way for nanophotonic quantum information applications. We anticipate that metasurfaces will become a standard tool in future quantum optics and will be used extensively in photonic quantum information systems—for example, for performing state tomography (*36*). These ideas can be extended to implement hyper-entangled state generation by using multifunctional or multispectral metasurfaces (*29*). The generation and control of quantum photon states via metamaterials leads to many new ideas and directions, ranging from using metasurfaces to entangle two photons of different frequencies and OAMs to manipulating quantum states of photons emitted from quantum dots in an integrated fashion.

REFERENCES AND NOTES

1. J. B. Pendry, *Phys. Rev. Lett.* **85**, 3966–3969 (2000).
2. V. M. Shalaev, *Nat. Photonics* **1**, 41–48 (2007).
3. D. Schurig *et al.*, *Science* **314**, 977–980 (2006).
4. M. Silveirinha, N. Engheta, *Phys. Rev. Lett.* **97**, 157403 (2006).
5. I. Liberal, N. Engheta, *Nat. Photonics* **11**, 149–158 (2017).
6. Z. Bomzon, V. Kleiner, E. Hasman, *Opt. Lett.* **26**, 1424–1426 (2001).
7. Z. Bomzon, G. Biener, V. Kleiner, E. Hasman, *Opt. Lett.* **27**, 1141–1143 (2002).
8. A. V. Kildishev, A. Boltasseva, V. M. Shalaev, *Science* **339**, 1232009 (2013).
9. A. Pors, O. Albrektsen, I. P. Radko, S. I. Bozhevolnyi, *Sci. Rep.* **3**, 2155 (2013).
10. X. Yin, Z. Ye, J. Rho, Y. Wang, X. Zhang, *Science* **339**, 1405–1407 (2013).
11. N. Yu *et al.*, *Science* **334**, 333–337 (2011).
12. D. Lin, P. Fan, E. Hasman, M. L. Brongersma, *Science* **345**, 298–302 (2014).
13. K. E. Chong *et al.*, *Nano Lett.* **15**, 5369–5374 (2015).
14. A. Arbabi, Y. Horie, M. Bagheri, A. Faraon, *Nat. Nanotechnol.* **10**, 937–943 (2015).
15. A. I. Kuznetsov, A. E. Miroshnichenko, M. L. Brongersma, Y. S. Kivshar, B. Luk'yanchuk, *Science* **354**, aag2472 (2016).
16. T. Roger *et al.*, *Nat. Commun.* **6**, 7031 (2015).
17. M. Siomau, A. A. Kamli, A. A. Moiseev, B. C. Sanders, *Phys. Rev. A* **85**, 050303 (2012).
18. L. K. Grover, *Proc. Twenty-eighth Annu. ACM Symp. Theory Comput. ACM*, 212–219 (1996).
19. P. W. Shor, *Proc. 35th Annu. Symp. Found. Comput. Sci. IEEE*, 124–134 (1994).
20. D. Deutsch, R. Jozsa, *Proc. R. Soc. Lond. A* **439**, 553–558 (1992).
21. B. G. Englert, C. Kurtsiefer, H. Weinfurter, *Phys. Rev. A* **63**, 032303 (2001).
22. A. Mair, A. Vaziri, G. Weihs, A. Zeilinger, *Nature* **412**, 313–316 (2001).
23. J. Leach *et al.*, *Science* **329**, 662–665 (2010).
24. L. Shi, E. J. Galvez, R. R. Alfano, *Sci. Rep.* **6**, 37714 (2016).
25. J. W. Silverstone *et al.*, *Nat. Photonics* **8**, 104–108 (2014).
26. M. Kues *et al.*, *Nature* **546**, 622–626 (2017).
27. E. Altewischer, M. P. van Exter, J. P. Woerdman, *Nature* **418**, 304–306 (2002).
28. M. S. Tame *et al.*, *Nat. Phys.* **9**, 329–340 (2013).
29. E. Maguid *et al.*, *Light Sci. Appl.* **6**, e17027 (2017).
30. M. V. Berry, *Proc. R. Soc. London Ser. A* **392**, 45–57 (1984).
31. K. Y. Bliokh, F. J. Rodríguez-Fortuño, F. Nori, A. V. Zayats, *Nat. Photonics* **9**, 796–808 (2015).
32. K. Y. Bliokh, F. Nori, *Phys. Rep.* **592**, 1–38 (2015).
33. E. Nagali *et al.*, *Phys. Rev. Lett.* **103**, 013601 (2009).
34. Materials and methods are available as supplementary materials.
35. D. F. V. James, P. G. Kwiat, W. J. Munro, A. G. White, *Phys. Rev. A* **64**, 052312 (2001).
36. K. Wang *et al.*, *Science* **361**, 1104–1108 (2018).

ACKNOWLEDGMENTS

The authors thank the group of Y. Silberberg from Weizmann Institute of Science, Israel, for the use of their 404-nm laser. **Funding:** The authors gratefully acknowledge financial support from the U.S. Air Force Office of Scientific Research (FA9550-18-1-0208), through their program on photonic metamaterials, and the Israel Science Foundation (ISF). The fabrication was performed at the Micro-Nano Fabrication & Printing Unit (MNF&PU), Technion. **Author contributions:** All the authors contributed substantially to this work. **Competing interests:** The authors declare no competing interests. **Data and materials availability:** All data necessary to support this paper's conclusions are available in the supplementary materials.

SUPPLEMENTARY MATERIALS

www.sciencemag.org/content/361/6407/1101/suppl/DC1
Materials and Methods
Supplementary Text
Fig. S1
Table S1
References (*37*–*39*)

17 April 2018; accepted 17 July 2018
10.1126/science.aat9042

Downloaded from http://science.sciencemag.org/ on September 16, 2018

Science

Quantum entanglement of the spin and orbital angular momentum of photons using metamaterials

Tomer Stav, Arkady Faerman, Elhanan Maguid, Dikla Oren, Vladimir Kleiner, Erez Hasman and Mordechai Segev

Science **361** (6407), 1101-1104.
DOI: 10.1126/science.aat9042

Going quantum with metamaterials

Metasurfaces should allow wafer-thin surfaces to replace bulk optical components. Two reports now demonstrate that metasurfaces can be extended into the quantum optical regime. Wang *et al.* determined the quantum state of multiple photons by simply passing them through a dielectric metasurface, scattering them into single-photon detectors. Stav *et al.* used a dielectric metasurface to generate entanglement between spin and orbital angular momentum of single photons. The results should aid the development of integrated quantum optic circuits operating on a nanophotonic platform.

Science, this issue p. 1104, p. 1101

ARTICLE TOOLS http://science.sciencemag.org/content/361/6407/1101

SUPPLEMENTARY MATERIALS http://science.sciencemag.org/content/suppl/2018/09/12/361.6407.1101.DC1

RELATED CONTENT http://science.sciencemag.org/content/sci/361/6407/1104.full

REFERENCES This article cites 35 articles, 10 of which you can access for free
http://science.sciencemag.org/content/361/6407/1101#BIBL

PERMISSIONS http://www.sciencemag.org/help/reprints-and-permissions

Use of this article is subject to the Terms of Service

Science (print ISSN 0036-8075; online ISSN 1095-9203) is published by the American Association for the Advancement of Science, 1200 New York Avenue NW, Washington, DC 20005. 2017 © The Authors, some rights reserved; exclusive licensee American Association for the Advancement of Science. No claim to original U.S. Government Works. The title *Science* is a registered trademark of AAAS.

Downloaded from http://science.sciencemag.org/ on September 16, 2018